fibers

MDPI

Article

The Effect of Projectile Nose Shape on the Critical Velocity of High-Performance Yarn

Boon Him Lim [1], Jou-Mei Chu [1], Jinling Gao [1], Benjamin Claus [1], Yizhou Nie [1] and Wayne Chen [1,2,*]

[1] School of Aeronautics and Astronautics, Purdue University, West Lafayette, IN 47907, USA; blim@purdue.edu (B.H.L.); chu82@purdue.edu (J.-M.C.); gao468@purdue.edu (J.G.); bclaus@purdue.edu (B.C.); nie14@purdue.edu (Y.N.)

[2] School of Materials Engineering, Purdue University, West Lafayette, IN 47907, USA

* Correspondence: wchen@purdue.edu; Tel.: +1-765-494-1788

Received: 3 March 2019; Accepted: 28 March 2019; Published: 3 April 2019

Abstract: In this study, ballistic experiments were performed to determine the critical velocity of a Twaron® 2040 high-performance yarn transversely impacted by round projectiles. Four different round projectiles possessing a radius of curvature of 2 μm, 20 μm, 200 μm and 2 mm were used in this study. Load cells were mounted to the grips to measure the load history of the yarn upon impact. A high-speed camera was incorporated into the ballistic experimental setup to capture the failure process of the yarn upon impact. A scanning electron microscope was utilized to perform post-mortem failure analysis on the recovered specimens. The results showed that as the radius of curvature of the projectile increased, the critical velocity also increased. The critical velocities for all cases were bounded between those predicted from the Euler–Bernoulli beam and Smith models. Upon impact above the upper limit of the critical velocity, the axial loads revealed a demonstrative reduction. The failure surfaces changed from shear to fibrillation as the radius of curvature increased. For those specimens that failed in shear, Hertzian contact model was used to predict the critical velocity.

Keywords: high-performance fiber; critical velocity; ballistic experiments; projectile nose shape; Smith theory

1. Introduction

Projectile nose shape is an important parameter that dominates the ballistic performance of a high-performance fiber [1–3]. The projectile striking velocity that causes instantaneous rupture on a yarn under transverse impact is defined as critical velocity [2,3]. Upon impact below the critical velocity, the transverse waves developed in the yarn deform according to the Smith theory [3–5]. Such transverse speed can be determined analytically using the projectile's striking velocity and the axial mechanical properties of the yarn [3–5]. On the other hand, if the projectile strikes above the critical velocity, the transverse displacement of the yarn is insignificant [2,6]. Additionally, even though the Smith theory is capable of predicting the critical velocity, the predicted results are always overestimated compared to those obtained from experiments [2,6–8].

A factor that causes the overestimation of the predicted critical velocity by the Smith theory is the projectile's nose shape [1,2]. Hudspeth et al. [2] shot a razor blade, a 0.30-cal fragmented simulation projectile (FSP) and a 0.30-cal round onto high-performance yarns and found out that the 0.30-cal round had the highest critical velocity, followed by the 0.30-cal FSP and the razor blade. The failure surface of the recovered specimens indicated that the yarns impacted by the razor blade failed in shear and the 0.30-cal round failed in fibrillation [2]. Multi-axial load developed in the yarn during transverse impact caused stress concentration and ultimately influenced the critical velocity [9].

Carr [10] shot a spherical steel projectile with a mass of 0.68 g onto para-aramid yarns and Dyneema® yarn. The failure surfaces of para-aramid yarns showed fibrillation irrespective of projectile's striking velocity [10]. However, for Dyneema® yarn, the failure was caused by shear when impacted below the critical velocity [10]. The failure surfaces for Dyneema® yarn revealed melting when impacted above the critical velocity which was similar to those observed by Hudspeth et al. [2,10].

Utomo et al. [7,11] performed single fiber aramid and ultra-high weight molecular Polyethylene (UHMWPE) impact experiments using saddle and cylindrical projectiles impacted to obtain the mechanical behavior. The results showed that the tensile modulus was independent of the projectile's striking velocity. The failure strains determined from the saddle projectile were higher than those obtained from the cylindrical projectile. However, both failure strains were lower than the quasi-static ultimate tensile strain [7].

Phoenix et al. [1] performed ballistic experiments on Dyneema® SK76 yarns with various initial pretension using two types of projectiles (flat and saddle noses). The results showed that as the initial pretension increased, the Young's modulus also increased. The critical velocity for the flat nosed projectile was lower compared to that of the saddle nose projectile. A wave-propagation model was developed to predict the critical velocity for a flat nose projectile impacted onto yarns with various initial pretension.

To the best of our knowledge, the circular nose shape projectiles (round, saddle or spherical) used in most of the transverse impact experiments contained only one radius of curvature [1,7,8,10,11]. The only exception was the experimental work done by Hudspeth et al. [2] where a razor blade and a 0.30-cal round projectile were used. The razor blade used in their study can be considered as a round projectile with a radius of curvature of 1.15 µm [2]. The difference in radius of curvature between the razor blade and the 0.30-cal round was at least 3 orders of magnitude. To understand the effect of projectile radius of curvature on the critical velocity, we performed ballistic experiments to determine the critical velocity of an aramid yarn transversely impacted by round projectiles with different radii of curvatures.

2. Materials and Methods

The aramid yarn specimens used in this study were strands of Twaron® 2040 yarns (Teijin Aramid, Conyers, GA, USA) extracted from plain weave single ply CT 709 Twaron® (Teijin Aramid, Conyers, GA, USA) in the warp direction. According to the manufacturer, this yarn consists of 1000 filaments with an average diameter of 9 µm. The quasi-static axial mechanical properties of the yarn were determined in a previous study [12]. The average Young's modulus, ultimate tensile strength and ultimate tensile strain were 92.55 ± 1.66 GPa, 2.47 ± 0.08 GPa and 2.71 ± 0.08%, respectively [12].

Ballistic Experiments

A gas/powder gun setup was utilized to perform the ballistic experiments to determine the critical velocity of the yarn, as shown in Figure 1.

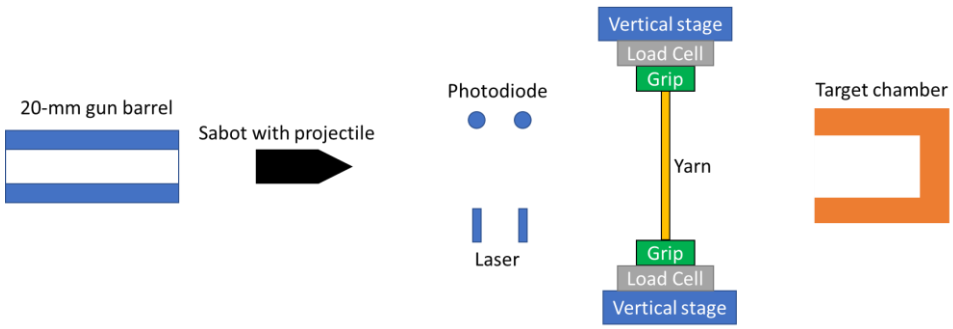

Figure 1. Experimental apparatus to determine the critical velocity.

The detail of the experimental setup, including the method to attach the yarn, was presented in previous studies [6,12]. The load cells were mounted to the grips to measure the load history. Four different types of round projectiles were used in this study. These were razor blades, 20-µm, 200-µm, and 2-mm round projectiles. The razor blades used were commercially available razor blades. In the previous study, scanning electron microscopy (SEM) images revealed that the average radius of curvature of the razor blade was 2 µm [12]. The remaining three projectiles were custom-made projectiles. The inner diameter of the gun barrel was larger than the projectiles. To fit these projectiles into the barrel, sabots were used, as shown in Figure 2.

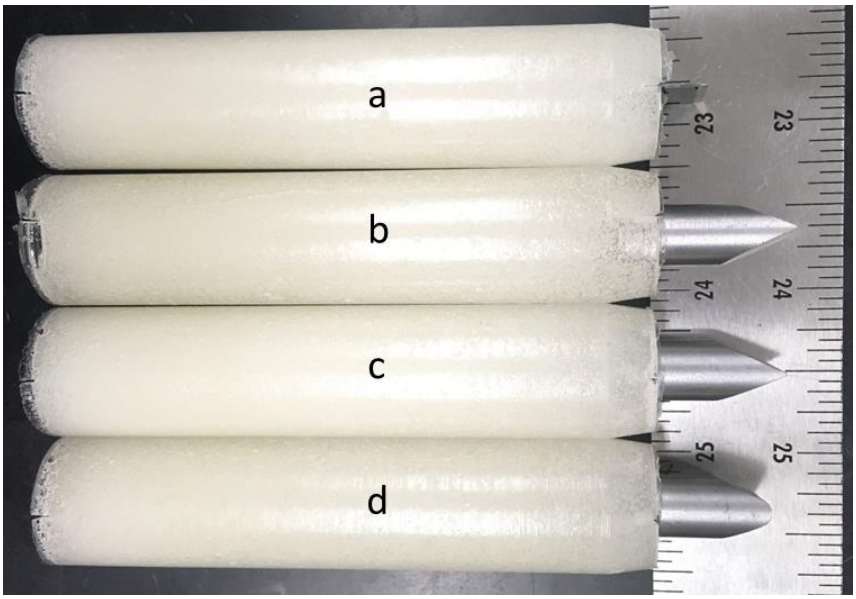

Figure 2. Round projectiles with a radius of curvature of (**a**) 2 µm, (**b**) 20 µm, (**c**) 200 µm and (**d**) 2 mm.

The sabots were made by polyurethane cast into a mold. An insert with a 9-mm hex shape was placed on top of the mold to fit different size projectiles except for the razor blade, as shown in Figure 2. A slot was cut at the top of each sabot using a precision wafering saw. For the razor blade, the purpose of this slot was to allow the razor blade to be placed on top of the sabot, as shown in Figure 2a. For the other types of projectiles, this slot was used to align the projectile to the sabot. These projectiles were then secured on the sabot with cyanoacrylate adhesive. Another parallel cut was made at the rear end of the sabot to assist in alignment of the sabot inside the gun barrel and to ensure the contact angle between the blade and the yarn was perpendicular. The combination of sabot and projectile yielded an average mass of 29 g for razor blade and 39 g for the other three types of projectiles. To observe the failure process of the yarn under transverse impact, a high-speed camera was integrated into the experimental setup.

3. Results

The critical velocities of Twaron 2040 yarns upon transverse impact by four round projectiles were obtained via ballistic experiments. It is important to emphasize that for a given case, the critical velocity has a range. If the impact of the projectile on the yarn was below the lower limit of the critical velocity, the transverse waves would develop and propagate in the yarn, causing it to deform according to Smith theory [3,6]. On the other hand, if impacted above the upper limit, the yarn would rupture instantaneously [2,6]. When impacted within the range of the critical velocity, some of the fibers would rupture upon impact and the remaining fibers would deform into a triangular shape as describe by Smith theory [2,3,6]. Therefore, when a yarn is transversely impacted by a projectile, the initial deformation of the yarn falls into one of the three possible cases: (i) no rupture, (ii) partial rupture, and (iii) instantaneous rupture [2,6].

Figures 3–5 show the high-speed images when impacted below, between and above the critical velocities by 20 μm, 200 μm and 2 mm round projectiles. For those yarns impacted by the 2 μm round projectile, the high-speed images can be found in [6].

From Figures 3–5, it was observed that as the radius of curvature of the projectile increased, the initial deformation of the yarn appeared to follow the contour of the projectile, as opposed to triangular-shape deformation as described by Smith [3]. In addition, upon impact above the critical velocity, prior to rupture, the transverse displacement of the yarn increased as the projectile's radius of curvature increased, as shown in Figure 5. From Figure 5a, the transverse displacement of the yarn at failure was small and occurred at the point of impact. Subsequently, as shown in Figure 5c, when impacted by a 2-mm round projectile, the transverse displacement of the yarn was larger than those impacted by smaller radius of curvature projectiles. Furthermore, the failure also initiated from a point away from the tips of the projectile as pointed by the arrows in Figure 5c. Figure 6 presents the initial deformation of the yarn at various projectile striking velocity for all four cases.

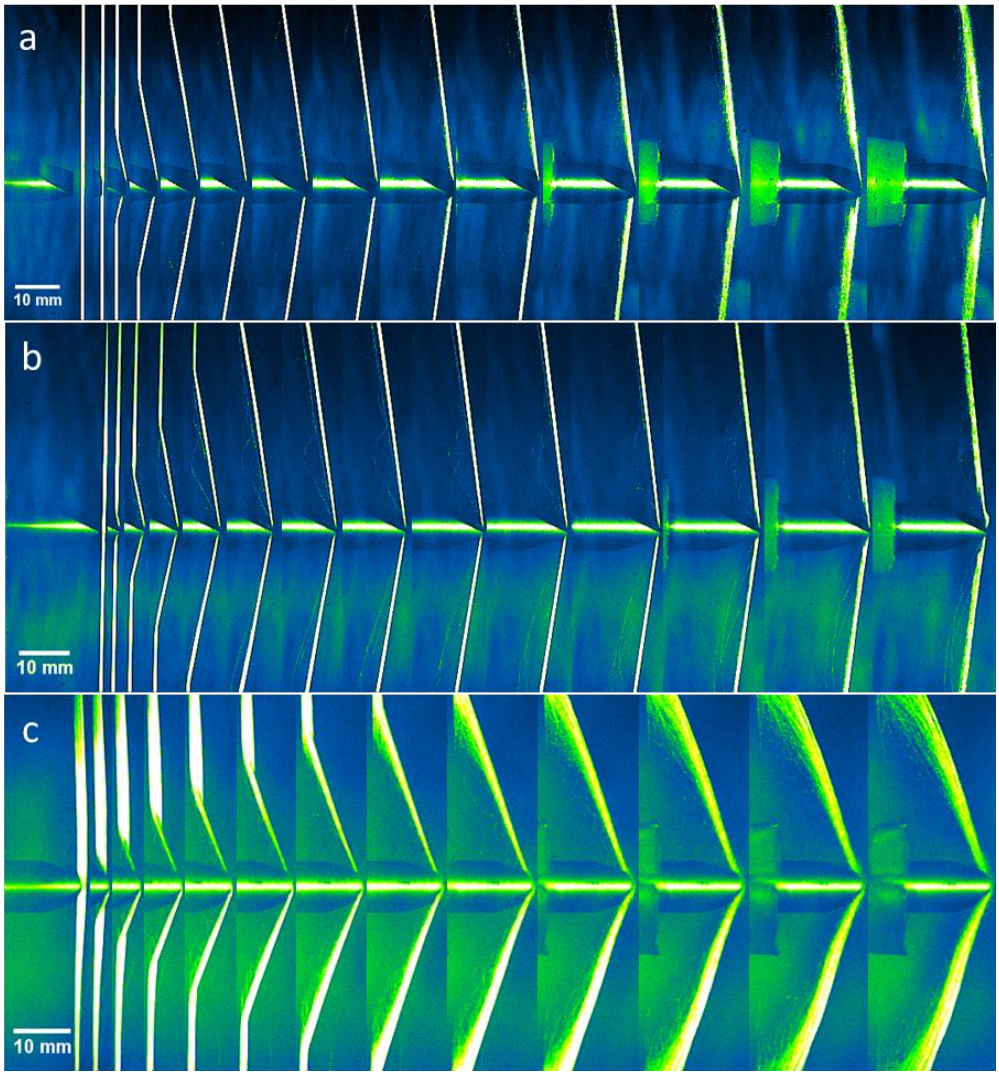

Figure 3. Deformation of yarn when transversely impacted by (**a**) 20 μm round, (**b**) 200 μm round and (**c**) 2 mm round projectiles at below the limit of their respective critical velocities. The projectile striking velocities were (**a**) 106 m/s, (**b**) 110 m/s and (**c**) 411 m/s. The time difference between each frame was (**a**) 20 μs, (**b**) 15 μs and (**c**) 4 μs.

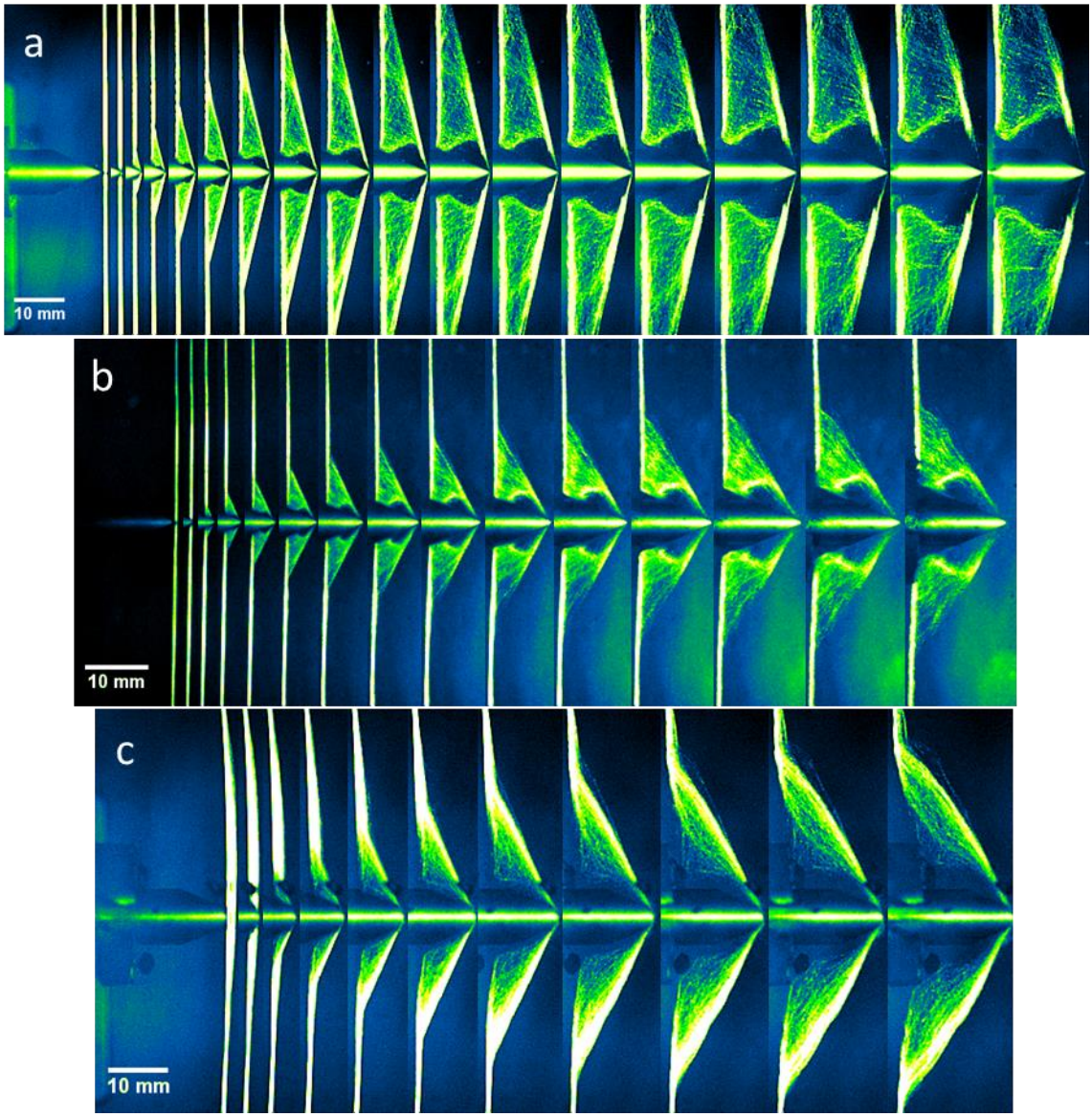

Figure 4. Yarn deformation when impacted by (**a**) 20 μm round, (**b**) 200 μm round and (**c**) 2 mm round projectiles between the limit of their respective critical velocities. The projectile stuck at (**a**) 218 m/s, (**b**) 458 m/s and (**c**) 474 m/s. The time difference between each frame was (**a**) 5 μs, (**b**) 2.5 μs and (**c**) 4 μs.

The range of critical velocities for Twaron® 2040 yarns transversely impacted by round projectiles possessing a radius of curvature of 2 μm, 20 μm, 200 μm and 2 mm were 83–186 m/s, 163–329 m/s, 183–525 m/s and 458–589 m/s, respectively. As pointed out in the previous study, the critical velocity predicted by Smith theory was around 731 m/s [3,6]. Such a discrepancy between the predicted and experimental critical velocities for all cases agreed with the results reported in the literature [1,2,7,8]. The load cells mounted to the grips allowed the force to be measured when the yarn specimen was subjected to transverse impact. Figure 7 plots the axial force at rupture versus the projectile striking velocity for Twaron® yarn impacted by 2 μm, 20 μm, 200 μm and 2 mm round projectiles. Such rupture load was obtained by averaging the loads from both load cells at failure.

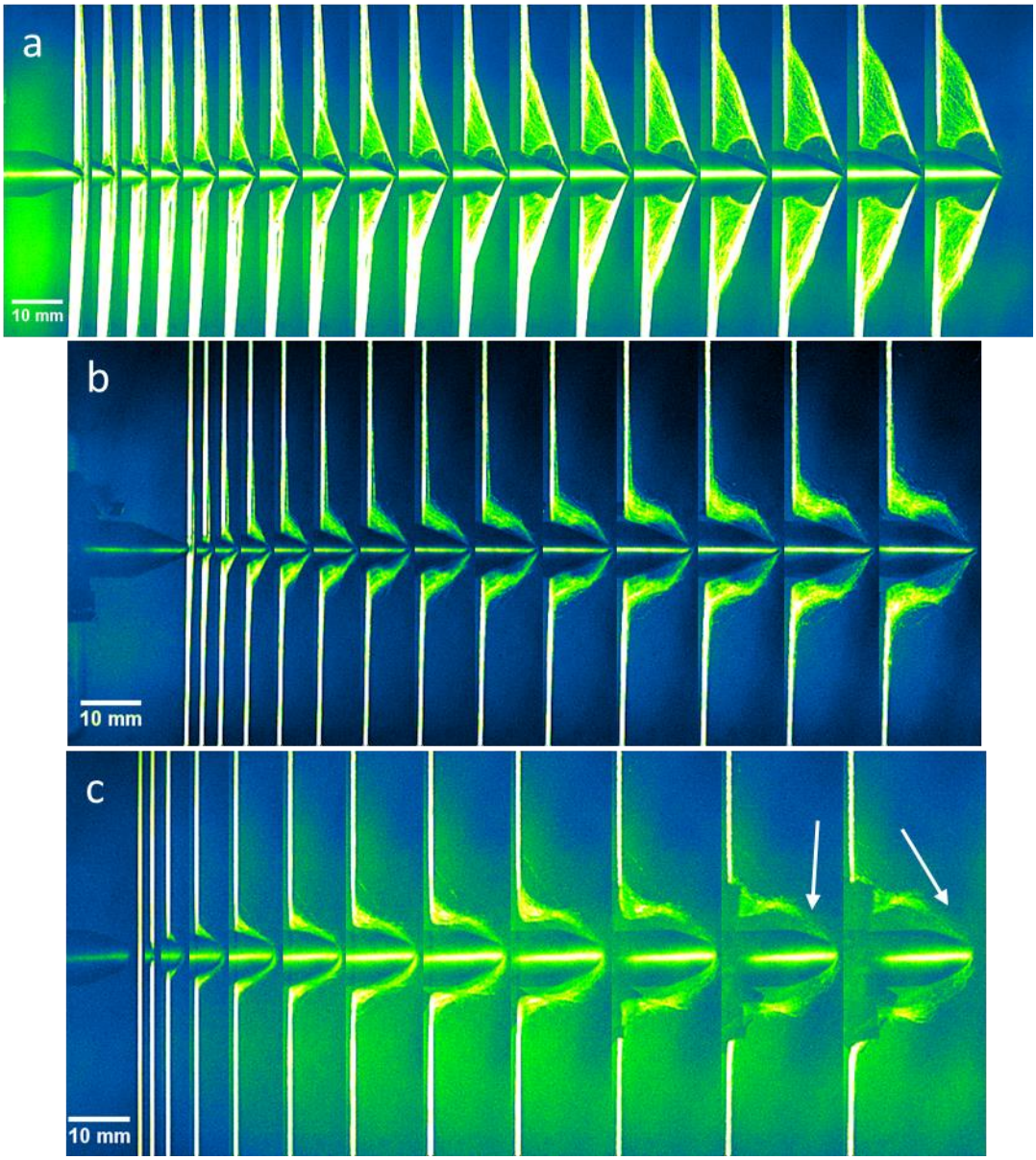

Figure 5. High-speed images when impacted by (**a**) 20 μm round, (**b**) 200 μm round and (**c**) 2 mm round projectiles above the critical velocity. The projectile stuck at (**a**) 343 m/s, (**b**) 552 m/s and (**c**) 649 m/s. The time difference between each frame was (**a**) 2 μs, (**b**) 2 μs and (**c**) 3 μs.

From Figure 7, it was observed that for a given striking velocity, the rupture load increased as the radius of curvature of the projectile increased. It is important to note that such rupture load is not equivalent to the axial load of the yarn when impacted below the lower limit of the critical velocity. The reason is that, upon transverse impact below the critical velocity, the yarn deformed into triangular shape causing the axial load in the yarn to have both vertical and horizontal components. Since the load cells were only capable of measuring the vertical force, the axial force in the yarn was underestimated. For 2 μm and 20 μm cases, the rupture loads decreased as the projectile striking velocity approached its respective lower limit of the critical velocity. A possible reason is that these small projectiles were able to shear through the yarns, causing them to fail progressively at the point of impact from projectile end toward the other free end. However, such failure process was not observed when impacted by larger round projectiles. The 2-mm round projectile was unable to shear through the yarn at low velocity, suggesting that the yarn failed due to stretching which caused the axial rupture load to be highest among all cases.

Unlike the previous case, when impacted above the upper limit of the critical velocity, the transverse displacement of the yarn was small. In addition, the yarn remained vertical away from the point of impact. Therefore, the measured loads represented the axial load in the yarn. The rupture load showed a demonstrative reduction when impacted above the critical velocity. This suggested that the load generated at the point of impact was unable to be transferred out by the stress waves, causing stress concentration to develop in the yarn and ultimately leading to premature failure [2,12–14].

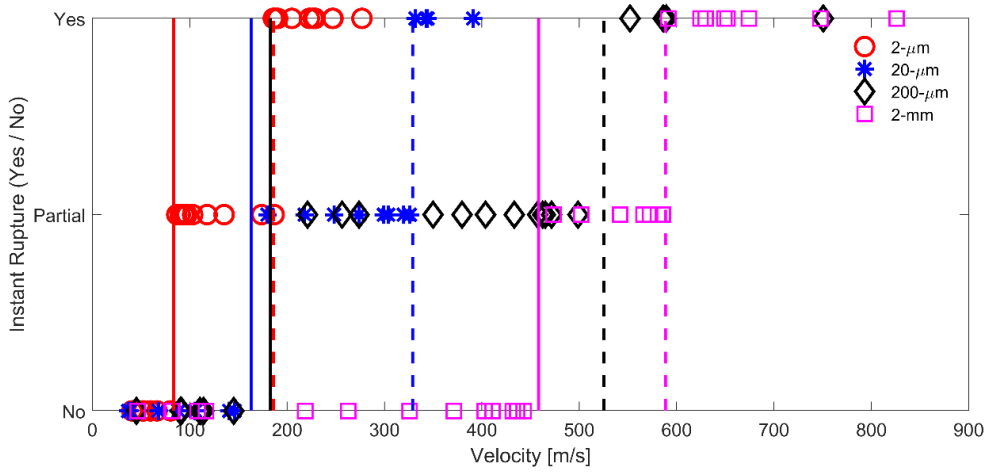

Figure 6. Yarn initial deformation when transversely impacted by (**a**) 2 μm round, (**b**) 20 μm round, (**c**) 200 μm round and (**d**) 2 mm round projectiles. Solid and dashed lines were the lower and upper limits of the critical velocities. The data for 2-μm round projectiles were adapted from [6].

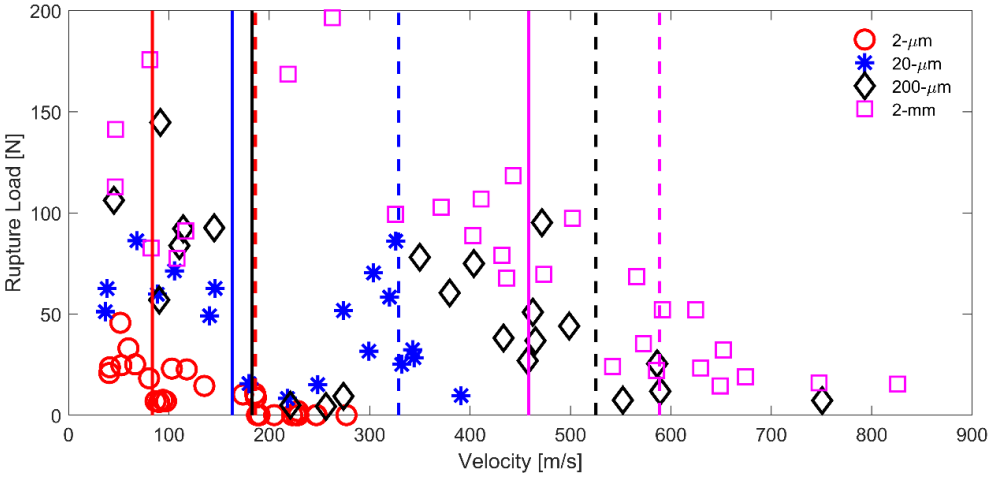

Figure 7. Axial load at rupture versus projectile striking velocity for a Twaron® 2040 yarn transversely impacted by (**a**) 2 μm round, (**b**) 20 μm round, (**c**) 200 μm round and (**d**) 2 mm round projectiles. Solid and dashed lines were the lower and upper limits of the critical velocities.

4. Discussion

In this section, the critical velocities predicted from several models will be compared to the experimental results. In additions, SEM was utilized to examine the failure surfaces of the recovered specimen.

4.1. Comparison between Experiments and Models

In the previous study, we used Euler–Bernoulli beam model and Hertzian contact model to improve the predictive capability of the critical velocity [6]. For the Euler–Bernoulli beam model, the yarn was modeled as a Euler–Bernoulli beam. An equation was formulated relating the transverse

particle velocity with the bending strain [6,15]. The critical velocity was then predicted by assuming the yarn failed instantaneously when the bending strain reached the ultimate tensile strain. For the Hertzian contact model, the projectile and yarn were modeled as a rigid sphere and Euler–Bernoulli beam respectively. The relationship between the contact load and deformation was described by the Hertzian contact theory [6,16]. By neglecting the fiber–fiber interactions and assuming the cross section of the yarn was circular, the critical velocity was predicted by assuming the projectile shear through the yarn when the indentation depth was equal to the diameter of the yarn. The detail formulation on both models can be found in [6]. Figure 8 shows the critical velocities obtained from experiments, Smith model, Euler–Bernoulli model and Hertzian contact model [3,6].

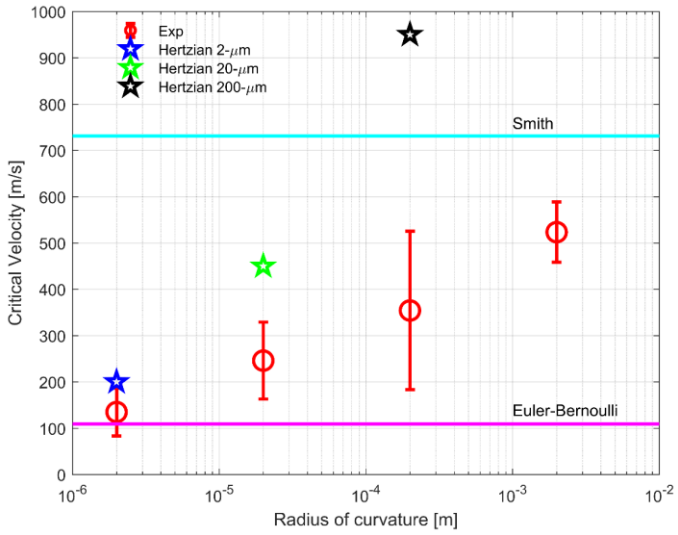

Figure 8. Critical velocities determined from experiments, Smith model [3,6], Euler–Bernoulli beam model [6] and Hertzian contact model [6]. The error bars represent the lower and upper limit of the critical velocities.

From Figure 8, it was observed that the average critical velocities from experimental results fall between those predicted by the Euler–Bernoulli beam and the Smith model. The major difference between these two models is that the Euler–Bernoulli beam model accounts for bending rigidity [6]. The Smith theory overestimated the critical velocities from 442% down to 40% as the projectile's radius of curvature increased from 2 µm to 2 mm. Conversely, the Euler–Bernoulli beam model underestimated the critical velocities from 79% to 19% as the projectile's radius of curvature decreased from 2 mm to 2 µm. These results suggested that the Euler–Bernoulli beam model can be used to predict the lowest limit of the critical velocity while Smith model can be used to predict the highest limit of the critical velocity. As pointed out from the previous study, the predicted critical velocities from the Euler–Bernoulli beam model and the Hertzian contact model agreed with those obtained from experiments for 2-µm round projectile, as shown in Figure 8 [6]. The same Hertzian contact theory was used to predict the critical velocity for a 20-µm and a 200-µm round projectiles impacted onto the Twaron® 2040 yarn. The predicted critical velocities were around 450 m/s and 950 m/s for 20-µm and 200-µm round projectiles, respectively. The error between the predicted critical velocities from the Hertzian model and experiments increased as the projectile radius of curvature increased. For the 200-µm case, the predicted critical velocity from the Hertzian model was higher than the Smith theory. SEM was used to perform post-mortem failure analysis on the failure surface of the recovered specimens.

4.2. Failure Surfaces

The images presented in this section were taken by an FEI Nova Nano SEM (FEI, Hillsboro, MA, USA) with an operating voltage, a spot size and an average working distance of 5 kV (HV), 3.5 and

5 mm, respectively. Figure 9 presents the failure surfaces of Twaron® 2040 yarns transversely impacted by a 2-µm round projectile.

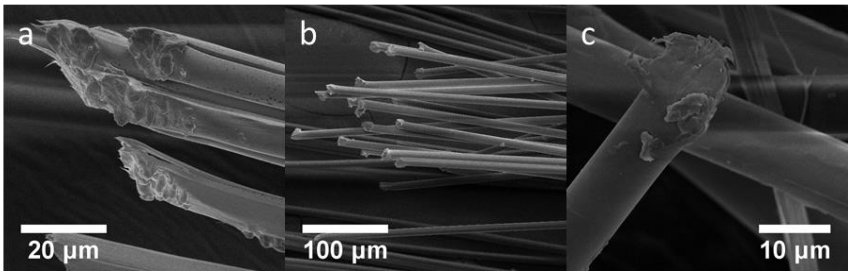

Figure 9. Failure surfaces of the recovered specimen transversely impacted by 2-µm round projectiles at (**a**) below, (**b**) between. and (**c**) above the critical velocities.

From Figure 9, it was observed that majority of the failure surfaces were flat. A small degree of fibrillation was observed when impacted below the critical velocities, as shown in Figure 9a. The failure surfaces suggested that the 2-µm round projectile was able to cut and shear through the fibers locally at the point of impact for all the velocities. Such a failure surface was observed at all projectile striking velocities, similar to those reported by Hudspeth et al. [2,13], Mayo and Wetzel [17] and Shin et al. [18].

When impacted by a 20-µm round projectile, the failure surfaces revealed a combination of shear and fibrillation, as shown in Figure 10. The combination mode suggested that the fibrils were first compressed in the transverse direction, causing the failure surface to be flat. The remaining fibrils were then stretched in the axial direction, causing them to fail in fibrillation. The failure criterion implemented in the Hertzian contact model required the indentation depth equal to the diameter of the yarn [6]. To satisfy this assumption, the fibers needed to fail in shear, causing the failure surfaces to be flat. A higher degree of fibrillation when impacted by 20-µm round projectile led to a larger error between the predicted critical velocity from the Hertzian model and experiments, as shown in Figure 8.

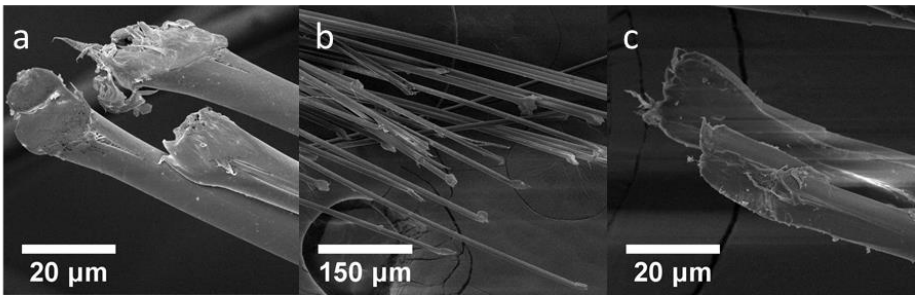

Figure 10. SEM images for 20-µm round projectiles impacted at (**a**) below, (**b**) between. and (**c**) above the critical velocities.

When impacted by 200-µm and 2-mm projectiles, the majority of the failure surfaces revealed fibril peeling on the fiber surface along the fiber direction as well as fibrillation, as shown in Figure 11. When impacted by these projectiles, the abrasion between fiber-projectile and fiber-fiber caused the fibrils to peel and create defects [19]. When the specimen exhibited stretching, these defects induced a shear stress in the specimen, causing the fibers to split axially which led to fibrillation [19]. The release of strain energy at failure caused fibrillation. The fibrils then snapped back and ultimately peeled off from that fiber [19]. As the radius of curvature of the projectile increased, a higher force was required to indent, causing shear failure in the fiber. For these two cases, the amount of force required to axially split these fibers was perhaps smaller than shear through the fiber. As a result, the fibers failed due to fibrillation. This fibrillation failure mode was also observed in the yarns upon quasi-static transverse loading with round projectiles possessing radii of curvatures larger than 1.59 mm and by Hudspeth

et al. in transverse impact experiments with a 3.81-mm round projectile onto a Kevlar® KM2 [2,12]. Since these specimens failed due to fibrillation, the Hertzian model was unable to accurately predict the critical velocity for these cases as the failure criterion required the specimens to fail in shear [6].

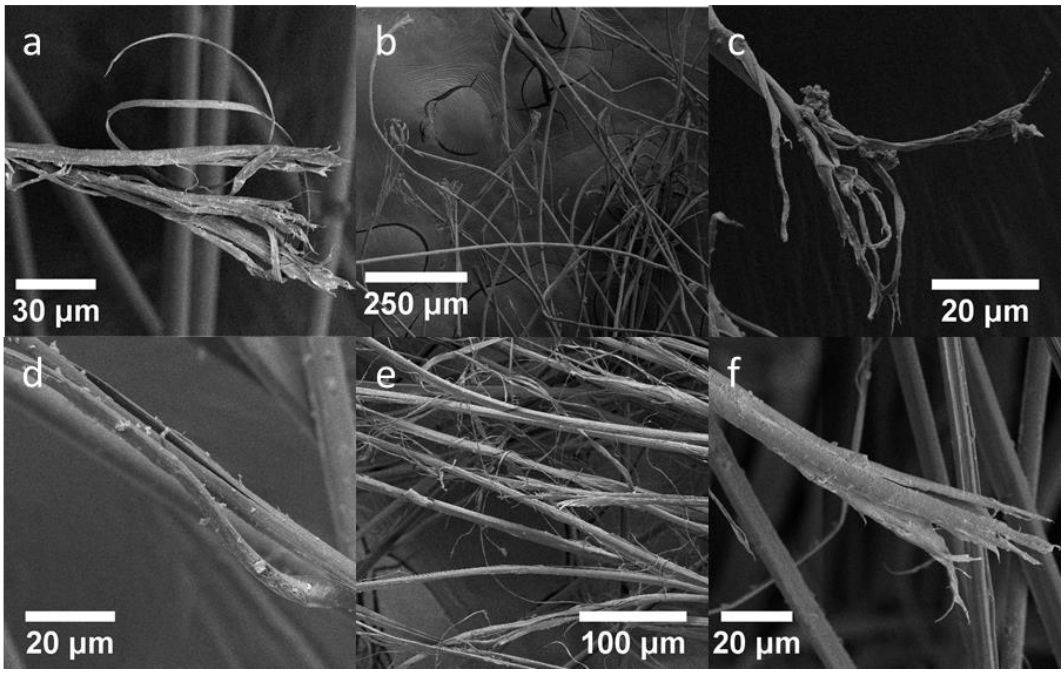

Figure 11. Failure surfaces for the recovered specimens transversely impacted by 200-μm round projectiles (first row) and 2-mm round projectile (second row) at below (**a**,**d**), between (**b**,**e**). And above (**c**,**f**) critical velocities.

5. Conclusions

Ballistic experiments were performed to determine the critical velocities for Twaron® 2040 yarns transversely impacted by round projectiles. Four different round projectiles possessing a radius of curvature of 2 μm, 20 μm, 200 μm and 2 mm were used in this study. The results show that the average critical velocities increase as projectile radius of curvature increases. These experimental critical velocities are bounded between those predicted from the Euler–Bernoulli beam and Smith models. The stress concentration developed at the point of impact caused the axial load showed a demonstrated reduction as the projectile struck above the critical velocities. The recovered specimens reveal that the failure surfaces change from shear to fibrillation as the projectile radius of curvature increases. For those specimens that were transversely impacted by 2 μm and 20 μm round projectiles, the majority of the fibers failed due to shear. As a result, Hertzian contact with shear failure criterion was able to predict their critical velocities.

Author Contributions: B.H.L., J.-M.C., J.G. and W.C. analyzed the results and contributed in discussion. J.G. perform failure surface analysis using SEM. B.H.L., J.-M.C., B.C. and Y.N. performed the experiments. W.C. supervised the project direction.

Funding: This research was funded by US Army PEO Soldier with a grant number W91CRB-14-C-0025. In addition, this research was partially sponsored by the Army Research Laboratory and was accomplished under Cooperative Agreement Number W911NF-12-2-0022.

Acknowledgments: The authors would like to express their gratitude to US Army PEO Soldier and Army Research Laboratory for providing the financial support for this work.

Conflicts of Interest: The authors declare no conflict of interest. The funding sponsors had no role in the design of the study; in the collection, analyses, or interpretation of data; in the writing of the manuscript, and in the decision to publish the results.

References

1. Phoenix, S.; Heisserer, U.; van der Werff, H.; van der Jagt-Deutekom, M. Modeling and Experiments on Ballistic Impact into UHMWPE Yarns Using Flat and Saddle-Nosed Projectiles. *Fibers* **2017**, *5*, 8. [CrossRef]
2. Hudspeth, M.; Chu, J.M.; Jewell, E.; Lim, B.; Ytuarte, E.; Tsutsui, W.; Horner, S.; Zheng, J.; Chen, W. Effect of projectile nose geometry on the critical velocity and failure of yarn subjected to transverse impact. *Textil. Res. J.* **2016**, *87*, 953–972. [CrossRef]
3. Smith, J.C.; McCrackin, F.L.; Schiefer, H.F. Stress-Strain Relationships in Yarns Subjected to Rapid Impact Loading: Part V: Wave Propagation in Long Textile Yarns Impacted Transversely. *Textil. Res. J.* **1958**, *28*, 288–302. [CrossRef]
4. Chocron, S.; Kirchdoerfer, T.; King, N.; Freitas, C.J. Modeling of fabric impact with high speed imaging and nickel-chromium wires validation. *J. Appl. Mech.* **2011**, *78*, 051007. [CrossRef]
5. Field, J.; Sun, Q. A high speed photographic study of impact on fibres and woven fabrics (from 19th International Congress on High-Speed Photography and Photonics 1990). *Spie Milest. Ser. MS* **1995**, *109*, 57–66.
6. Lim, B.; Chu, J.M.; Claus, B.; Nie, Y.; Chen, W. Critical Velocity of High-Performance Yarn Transversely Impacted by Razor Blade. *Fibers* **2018**, *6*, 95. [CrossRef]
7. Utomo, B.H.; Broos, J. Dynamic Material Determination Using Single Fiber Impact. In Proceedings of the a Conference & Exposition on Structural Dynamics (IMAC XXV), Orlando, FL, USA, 19–22 February 2007.
8. Bazhenov, S.; Dukhovskii, I.; Kovalev, P.; Rozhkov, A. The fracture of SVM aramide fibers upon a high-velocity transverse impact. *Polym. Sci. Ser. Vysokomol. Soedin.* **2001**, *43*, 61–71.
9. Hudspeth, M.C. Multi-Axial Failure of High-Performance Fiber during Transverse Impact. Ph.D. Thesis, Purdue University, West Lafayette, IN, USA, 2016.
10. Carr, D.J. Failure Mechanisms of Yarns Subjected to Ballistic Impact. *J. Mater. Sci. Lett.* **1999**, *18*, 585–588. [CrossRef]
11. Heru-Utomo, B. Dynamic Young's modulus determination using single fibre impact. In Proceedings of the 57th ARA Meeting, Venice, Italy, 30 April–4 May 2016; pp. 18–22.
12. Lim, B.H.; Chu, J.M.; Chen, W. Mechanical Behavior of High-Performance Yarns Transversely Loaded by Different Indenters. *Fibers* **2018**, *6*, 69. [CrossRef]
13. Hudspeth, M.; Li, D.; Spatola, J.; Chen, W.; Zheng, J. The effects of off-axis transverse deflection loading on the failure strain of various high-performance fibers. *Textil. Res. J.* **2016**, *86*, 897–910. [CrossRef]
14. Hudspeth, M.; Chen, W.; Zheng, J. Why the Smith theory over-predicts instant rupture velocities during fiber transverse impact. *Textil. Res. J.* **2015**, *86*, 743–854. [CrossRef]
15. Doyle, J.F. *Wave Propagation in Structure: Spectral Analysis Using Fast Discrete Fourier Transforms*; Springer: New York, NY, USA, 1997.
16. Popov, V.L. *Contact Mechanics and Friction*; Springer: New York, NY, USA, 2010.
17. JB Mayo, J.; Wetzel, E. Cut resistance and failure of high-performance single fibers. *Textil. Res. J.* **2014**, *84*, 1233–1246. [CrossRef]
18. Shin, H.S.; Erlich, D.C.; Simons, J.W.; Shockey, D.A. Cut Resistance of High-strength Yarns. *Textil. Res. J.* **2006**, *76*, 607–613. [CrossRef]
19. Hearle, J.W.; Lomas, B.; Cooke, W.D. *Atlas of Fibre Fracture and Damage to Textiles*; Elsevier: New York, NY, USA, 1998.